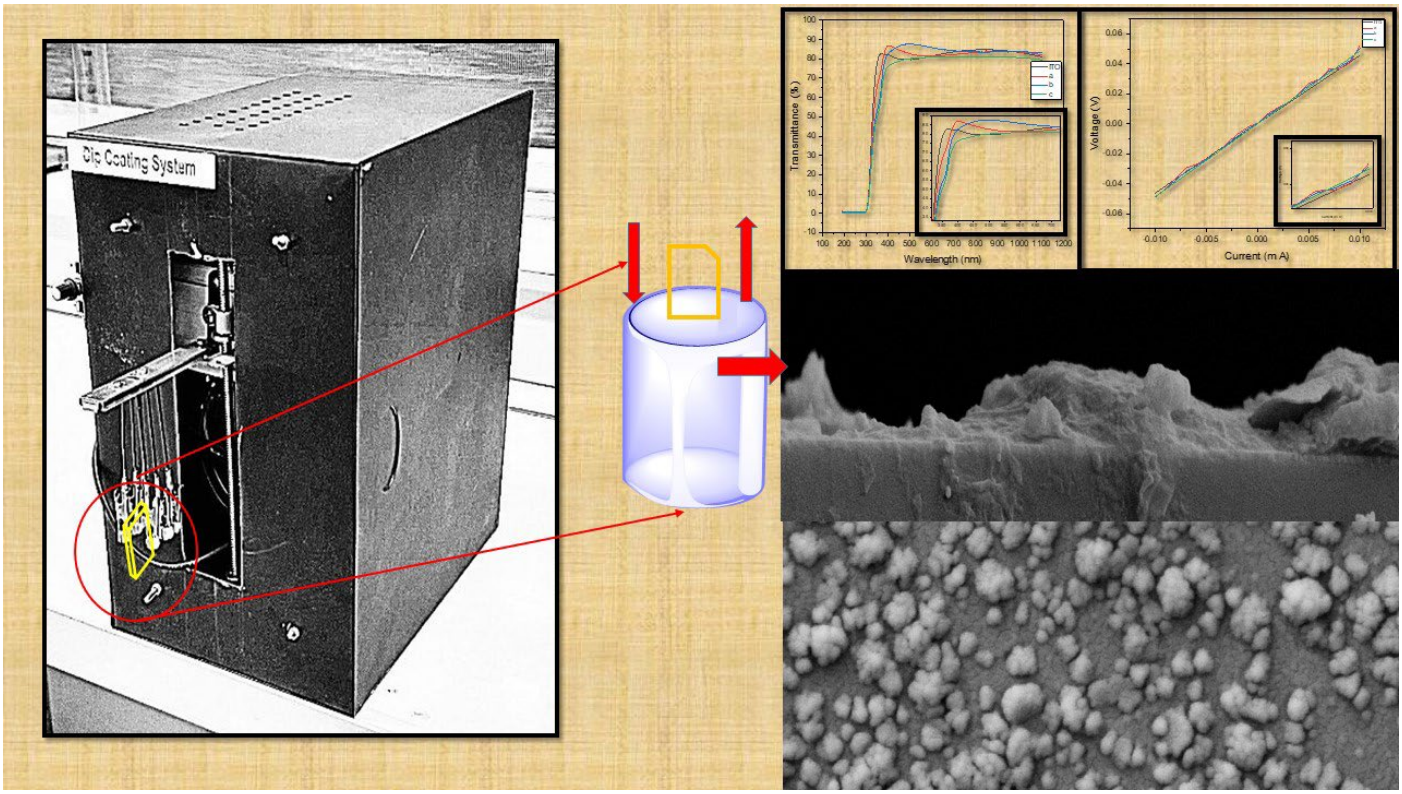

DESIGN AND FABRICATION OF A LOW-COST DIP COATING SYSTEM FOR DEPOSITING HOMOGENEOUS AND TRANSPARENT THIN FILMS

Asaad S. Yasir[1], Basheer M. Hussein[2], Ammar S. Hameed[1], Noor J. Ridha[1*], Firas K. Mohamad Alosfur[3], Khawla J. Tahir[1] and Rajaa A. Madlol[1]

[1] Department of Physics/ College of Science/ University of Kerbala, Kerbala, Iraq.

[2] Department of Physiology and Medical Physics/ College of Medicine/ University of Al-Ameed, Kerbala, Iraq.

[3] Department of Environmental Health, College of Applied Medical Sciences, University of Kerbala, Kerbala, Iraq.

* asaad.s@s.uokerbala.edu.iq

DESIGN AND FABRICATION OF A LOW-COST DIP COATING SYSTEM FOR DEPOSITING HOMOGENEOUS AND TRANSPARENT ZnO THIN FILMS

Abstract

ZnO has a resistivity of up to 10^4 Ω cm^{-1} in most cases. Nevertheless, by increasing the layer thickness, the resistivity decreases as well, resulting in greater current transport. The dip coating system was developed to prepare the ultra-thin film, it relied on a controller, stepper motor and some low-cost recycled materials. Thin films of ZnO were successfully deposited on indium tin oxide substrates. The effects of the dipping cycles were investigated. Dipping processes were applied several times (1, 2, and 3) for the same concentrations (0.1) M to obtain homogeneous thin films.

X-ray diffraction showed that the structure of ZnO is hexagonal Wurtzite. The crystals were in the nanoscale size range as (19.18, 24.76, and 31.29) nm. As for the examination by FESEM, it was found that homogeneous layers formed when increasing the number of times of coating for the prepared thin films. High transmittance, decreasing in energy gap, and suitable surface resistance ZnO thin films were achieved. In the wavelength range of 190 – 1100 nm, the thin films had an optical transmittance of up to 87%. The sheet resistance values were determined to be 19.202 Ω sq^{-1} indicating that the characteristics of ZnO thin films have improved. The dip coating device is designed to be easy to use, inexpensive and economic in terms of using the raw materials. This low-cost manufactured device contributes to scientific development for researchers who are unable to buy expensive devices that perform the same purpose and give the same results.

Keywords: dip coating, thin films, sol-gel, ZnO

INTRODUCTION

Recently, thin films have already been used in many devices, specifically, as transparent conducting electrodes (TCE) since they can be used in a wide range of applications [1]. Several materials could be used as TCE such as carbon nanotubes, graphene, and transparent conducting oxides (TCO) [2–4]. Semiconductors such as TiO_2, SnO_2, and ZnO are one of the most promising TCO since they exhibited high conductance and high transmittance properties. In particular, ZnO has been widely used as TCE since it has a direct wide bandgap of 3.3 eV, a large exciton binding energy (60 meV), and high electron mobility of (155 $cm^2 V^{-1}s^{-1}$) [5–8]. Techniques for preparing compounds containing zinc oxide play a great influence to obtain heterogeneous and multi-nano photocatalyst that rely heavily on zinc oxide to obtain new properties by means of heterogeneous junctions. There are many manufacturing methods for these nanocomposites based on zinc oxide and heterojunctions including hydro, and solvo-thermal technology, solution-based technology, microwave-assisted ultrasound, in situ assembly, electrospinning, pyrolysis, and chemical co-deposition[9]. These techniques improve the physical properties of the resulting compound, as they improve high-speed transmission of electrons in semiconductors and improve crystallization, nanostructure, phase and chemical properties, which leads to a significant increase in photocatalytic performance. The properties of the sol-gel method include higher homogeneity, adjustable stoichiometry, high purity, and flexibility in the fabrication of thin films[10]. Solvents have an effect on the dip coating process, the function of solvents is to act as carriers of solute, control viscosity for application and flow, aid in film formation, and hydrate substrates to aid in dispersion and adhesion. Important solvent properties include besides physical properties such as volatility, boiling point, surface tension, viscosity, resistance (electrical conductivity), cost, toxicity, flammability and odor. Surface tension has an effect in coatings on many properties such as coating wetting, dispersion, wetting of the substrate and spray ability. Low surfactant solvents can improve these properties and distribute additives[11]. The dip coating method has advantages and disadvantages, including (1) it is possible to paint both sides of the sample at the same time, while other methods cannot, (2) the large homogeneity of the resulting layers and there is no difference in coating large or small samples, but other methods face difficulty in that, (3) possibility of coating inside and outside pipes of different diameters and shapes and this is only possible with difficulty, (4) dip coating is scratch-resistant, solid and durable against environmental influences, (5) the process of dip coating is not economical when preparing a thin film for more than 15 layers because each layer must be heat treated, (6) this method is used only for oxides because metallic films are very difficult to produce, and (7) the properties of the thin film can only be measured after heat treatment[12–14].

Therefore, different deposition devices were designed to achieve the required properties of the prepared thin film [15]. There are many techniques that have been used for depositing thin films (in addition for the above) namely chemical vapor deposition (CVD) [16], laser ablation [17], thermal evaporation [18], electroplating [19], painting [20], sputtering [21], photodeposition[22], and spin coating [23,24]. Nowadays, the development of the

production of characteristic thin films has been hampered by preparation techniques that are either expensive or complicated. Furthermore, there are still certain challenges of large-scale production and the relatively high cost of deposition of sophisticated structures, such as quantum wells and wires. Thus, it is necessary to develop a low-cost depositing method suited for thin films with controlled thickness. Dip coating is a simple method for depositing thin films of different thicknesses ranging from several parts of the nanometer to the micrometer [25]. Oxide films make up the majority of dip coatings. Large panes of glass are the most common substrates that are removed from the solution and placed in a humid environment, solvent evaporation occurs. At high temperatures, numerous reactions occur before the clear oxide layer is created. It is possible to produce single oxides, crystalline and amorphous multicomponent oxides[12]. It is an effective system to produce thin films with controlled thickness with variable time and speed of film dragging [26]. The dip coating method offers several advantages such as larger coating size, a more efficient production process, and less amount of the required coated materials [27]. This technology is used in various types of industries including electronics, optics, and photosynthesis [28]. The dip coating device is essential for the production of high-quality thin films and is commercially available but unfortunately, it is expensive around (2000 – 4000) USD. Therefore, in this work, a low-cost and high-efficiency dip coating device was designed and fabricated from recycled materials to deposit homogeneous thin films. The fabricated dip coating system in this work has the advantages of being inexpensive and having the ability to simply modify the thin film thickness and properties.

MATERIAL AND METHODS

Dip coating design and fabrication

The current study focuses on the low-cost manufactured dip coating system used for preparing thin films , which includes a stepper motor (42HD2037 NEMA17 Stepper Motor 33 mm), (TB6600 Stepper driver module 4.5A), AC/DC adapter (JCY-1250) output 12 V—5 A, SK8 SH8 vertical type holder 8mm linear rail shaft end support, 626ZZ ball bearing, Copper nut for T8 Lead screw, Chrome plated smooth rod diameter 8 mm length 320 mm, flexible couplings 8 MM, T8 guide Lead screw 300 mm, and container. The stepper motor rotates the lead screw, which causes the coating arm to move downward or upward, figure (1) illustrates a diagram of the dip coating system.

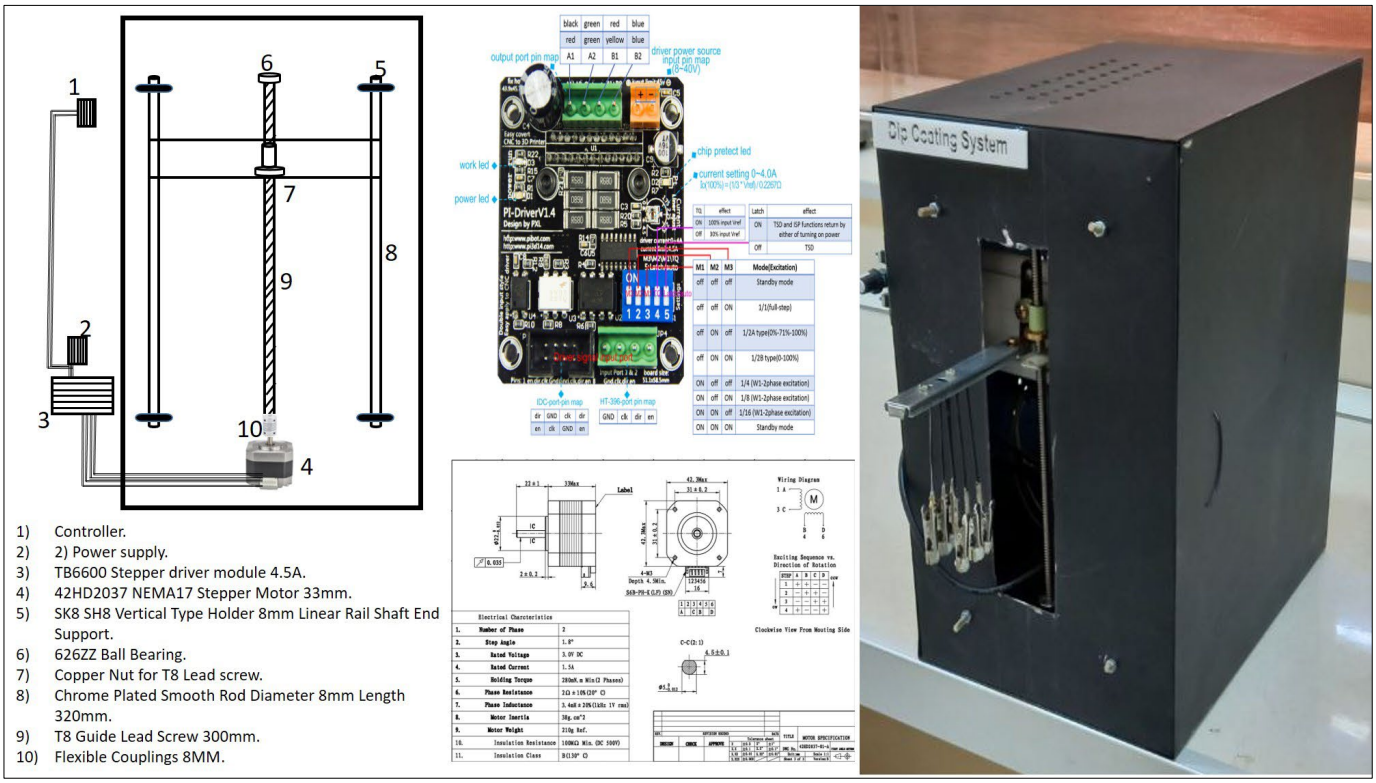

Figure (1). Schematic diagram of designed dip coating system.

The main forces influencing the dip coating process are inertia, solution viscosity, gravitational force, and liquid surface tightening [29]. To control the depositing of the dip coating system, a balance among these forces should satisfied. This could be achieved by modifying the speed of the motor which should be specified by controlling the time of the motor step, as well the immersion distance. The microprocessor controls the rotational speed of the stepper, which determines the speed of the dipping arm as it enters the coating liquid. A driver will be in charge of controlling the stepper motor's speed and direction of motion.

Stepper motions can be more exact with micro-step movements by adjusting the driver parameters. The device exhibited complete controlled parameters depending on the driver and the controller. The novelty of this work is that a smooth-moving by copper nut and T8 Lead screw was used which leads the stepper motor to be moved and gives a high flow of movement. Generally one of the drawbacks of this method is that it is considered a time-consuming method [30,31]. This problem was overcome by making a sample holder that can carry six samples at once (or more) to obtain 6 samples at the same time and with the same preparation conditions as shown in figure (2).

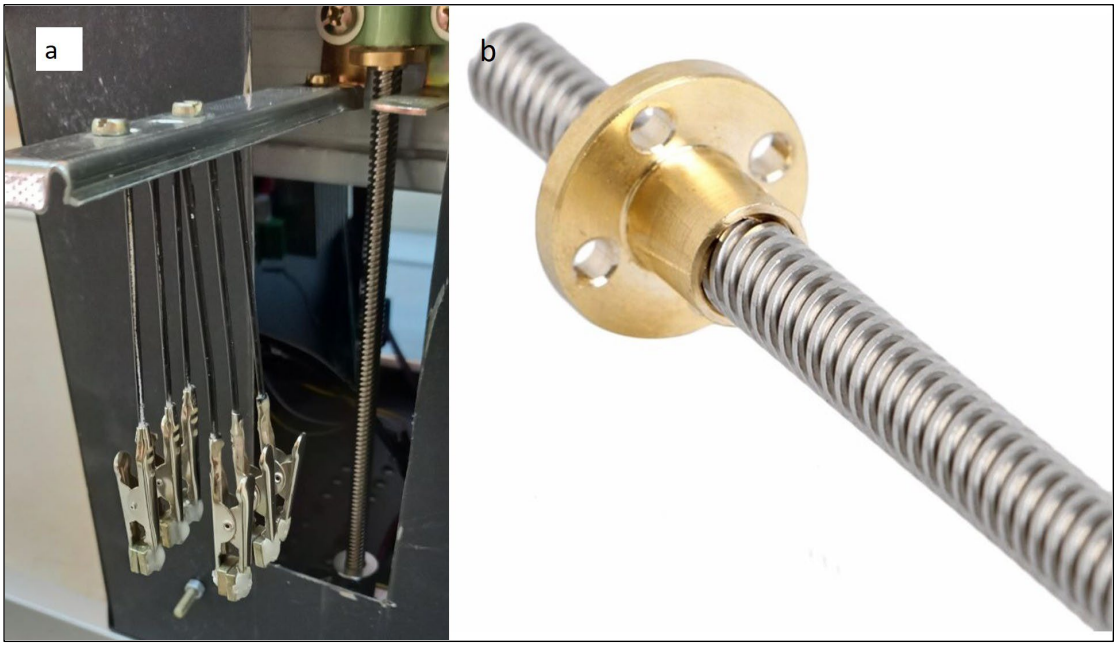

Figure (2). a) The developed sample holder, b) Copper nut and

T8 guide Lead screw 300 mm

Sample preparation

To prepare the coating material solution, zinc acetate dihydrate was dissolved in ethanol (viscosity 1.13 Pa.sec and ph = 6) with continuous stirring by magnetic stirrer for 60 minutes at 60 °C to obtain a homogeneous solution at concentration of (0. 1) M. This technique includes several consecutive steps, first immersing the substrate Indium Tin Oxide coated on glass (ITO) in a solution containing the coating material at a constant speed (10 mm s^{-1}), after which the substrate remains in the solution for a certain period (5 minutes) and then the substrates were pulled upwards at a constant speed (10 mm s^{-1}). There is a speed below which the substrate emerges from the bath unwetted, just as in the continuous process, if the liquid does not completely wet the substrate. On the other hand, if volatile components from the deposited film are evaporated quickly enough, it may increase the film's viscosity and prevent it from locally thinning, dewetting, or draining further before it solidifies. The film surface may prematurely solidify into a skin due to overly quick evaporation, which will slow down the subsequent drying process. After dragging the samples, they were dried at 90 °C for 10 minutes on the hot plate to evaporate the solvent to obtain an ultra-thin layer. Ambient temperature and humidity have an effect on the immersion coating process. In this work, when pull out the samples from the coating liquid, we put them on the hot plate during several seconds so that the surrounding conditions do not affect the drying of the sample during the drawing. These processes were repeated (1, 2, and 3) times to obtain three samples namely (a, b and c), respectively. Finally,

the samples were annealed in a muffle furnace for 60 minutes at 300 °C. The annealing process of samples with ITO or FTO substrate at a high temperature shall be greater than 300 °C, due to their high temperature tolerance and the fact that they do not contain a polymer. As for samples that contain a polymer or a plastic substrate, it is preferable to use laser annealing because it does not affect the plastic and is very fast. Excimer laser annealing (ELA) was previously used in place of thin film thermal annealing[32]. Laser annealing has good surface smoothness properties. As for the electrical resistance, if the laser is used with an excessively high or low energy, it affects increases of the resistance, so it will be very high.[33] The preparation procedure was illustrated in figure (3).

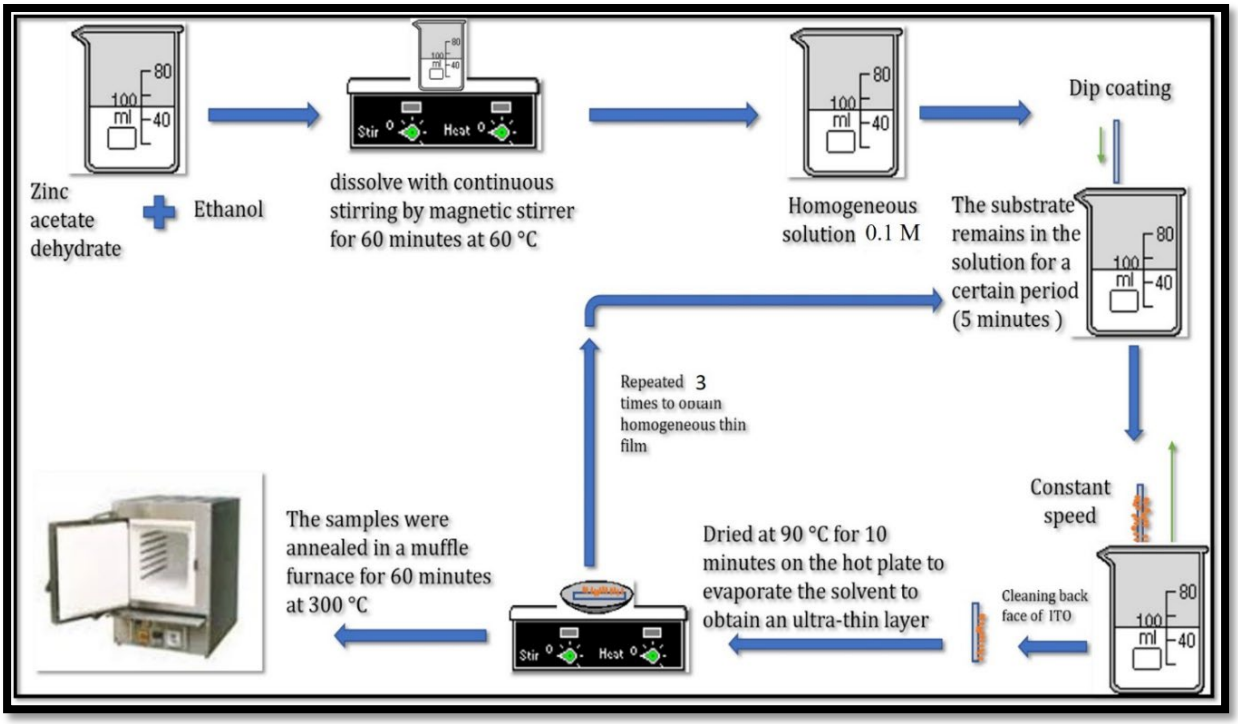

Figure (3). Schematic diagram of the sample preparation procedure.

Sample Characterization

Dip coating is a simple and inexpensive method for depositing thin layers. To deposit an oxide layer, the immersion, withdrawal speeds, dipping cycles, and solution viscosity may all be accurately controlled. To study the effect of the dipping times, the dipping was repeated (1, 2, and 3) times to obtain a suitable thickness of the prepared thin film. To evaluate the structural qualities of the thin films, XRD (Shimadzu /Japan) was used for characterizations. Field emission scanning electron microscopy (FESEM) was used to analyze the morphology and microstructure of the samples (EBSD instrument: ZEISS SIGMA VP/Germany). To examine the FESEM image using the Origin Lab tool and Image J to measure the

diameters of the zinc particles and how they are dispersed. To study the optical properties of the thin films, the characterizations were carried out using (Shimadzu-UV-VIS spectrophotometer (UV-1900i spectrophotometer). To examine the transparency of the prepared samples, the optical transmittance of the synthesized thin films was investigated. Also, to examine the transparency (a camera was used for captured photos from Samsung Galaxy A31, a primary 48-megapixel sensor, an 8-megapixel sensor with a wide-angle lens, a 5-megapixel depth camera, and a 5-megapixel macro camera). The electrical properties characterized in a four-point probe method using Keithley 2450 source meter and the applied current was ranged from (-10 to10) mA [34].

RESULTS AND DISCUSSION

Structural properties

To investigate the structure of the prepared thinfilms, XRD analysis was performed as shown in figure (4). When comparing the diffraction peaks and the JCPDS data (96-900-8878), it was found that the prepared material shows hexagonal zinc oxide (P 63 mc) structure. The lattice constants of ZnO are a = b = 3.25 Å and c = 5.207 Å. Generally, five main peaks were detected namely, (100), (002), (102), (103), and (202) which belong to the hexagonal Wurtzite structure. The highest intensity was the plain (100) at angle 2Θ = 31.767° which represents the preferred direction. These results which detected by XRD data proved that the deposited samples were pure which show the effectiveness of the manufactured dip coating system for depositing pure thinfilms.

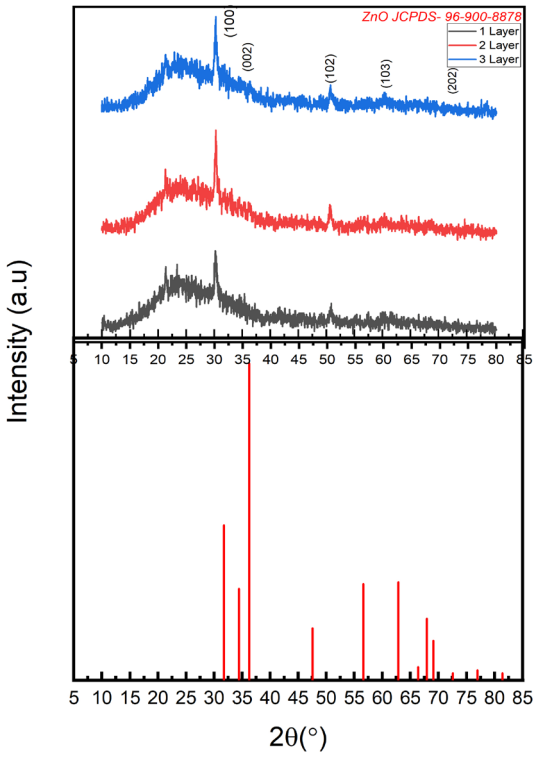

Figure (4). XRD patterns and slandered JCPDS data.

In order to ascertain the effect of dipping times on the thickness, morphology and topography of the prepared thinfilms, FESEM studies were conducted. Figure (5 a, b, and c) show the cross section of 1, 2, 3 layers, respectively. As for the single-layer sample, figure (5a) the thickness was 133 nm. By increasing the dipping time to 2 times as shown in figure (5b) the thickness was increased to 465 nm. Finally, by increasing the dipping times to 3 times, as in figure (5c) the thickness become 497nm. These results indicated that increasing the dipping time is an effective way to control the thickness. Figure (5 d, e and f) represents the top-view of the prepared samples. It is clear that after annealing, the ZnO particles aggregated to be of this shape. When coating for the second time, these voids were filled and a homogeneous layer was formed, as shown in figure (5 e). As for the third layer, the average crystal size is greater than that of the second layer, and it is also homogeneous, figure (5 f).

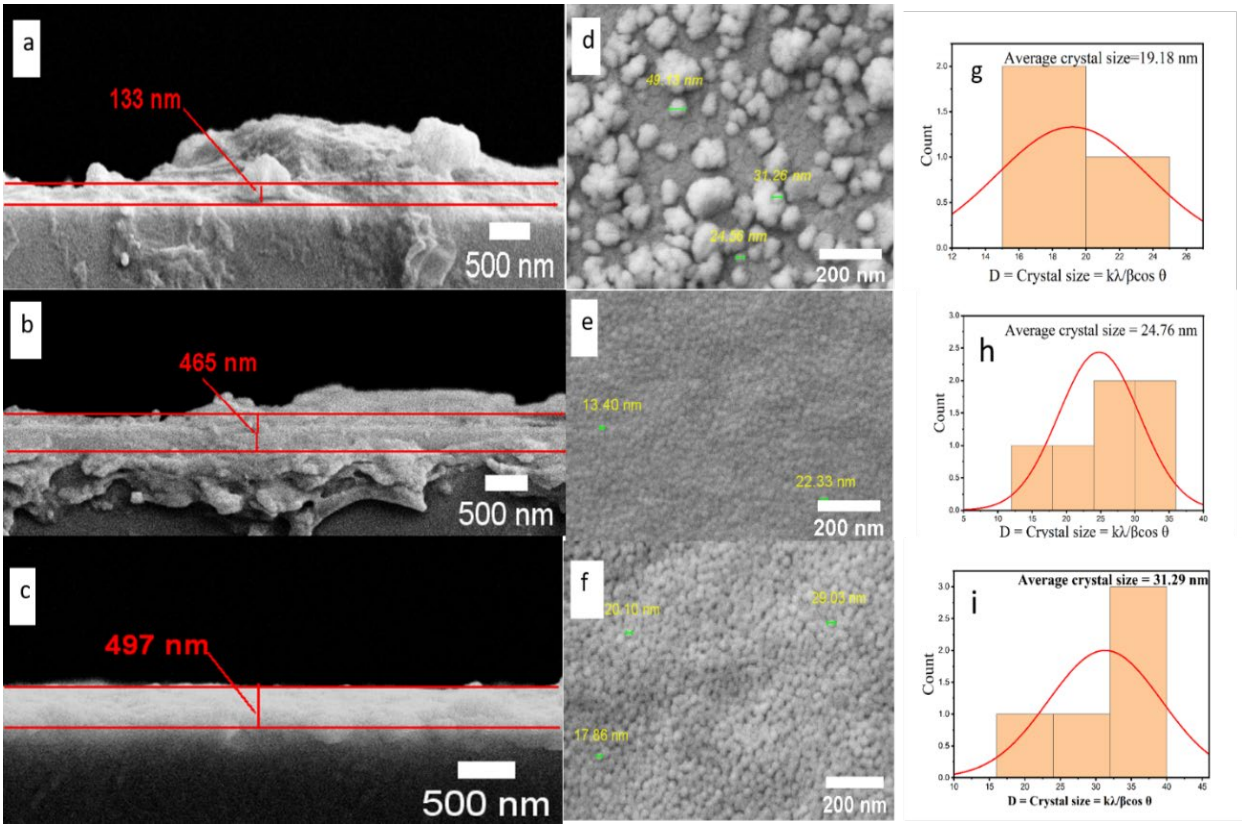

Figure (5). Images (a, b, and c) cross section, (d, e, and f) FESEM top-view, (g, h, and i) particles size of samples1, 2, and 3 layer respectively.

The average crystal size of the samples was calculated from the XRD data using Scherrer equation:

$$D = \frac{k\lambda}{\beta \cos\theta} \quad (1)$$

$$\delta = 1/D^2 \quad (2)$$

$$\varepsilon = \beta / (4*\tan(\theta)) \quad (3)$$

Where D is crystal size, k is Scherrer constant (0.9), λ is the wave length for X-ray source (1.5406nm), β is full width at half maximum (FWHM), and θ is peak position, δ is dislocation density, and ε is micro strain. It was found that the first layer has an average crystal size of about 19.18 nm, the second layer is about 24.76 nm, and it is about 31.29 nm for the three-layer sample, as shown in table (1).

Table (1). Illustrate all parameters calculated from XRD data.

Sample ID	2θ (°)	β (°)	λ (nm)	k	D (nm)	Average crystal size (nm)	$\delta *10^{-3}$ $(nm)^{-2}$	$\varepsilon * 10^{-3}$
1 Layer	21.41	0.51	0.15406	0.9	15.92	19.180	3.94	11.72
	30.19	0.34	0.15406	0.9	24.31		1.69	5.48
	50.63	0.51	0.15406	0.9	17.31		3.34	4.68
2 Layer	21.27	0.25	0.15406	0.9	31.84	24.76	0.99	5.90
	30.27	0.34	0.15406	0.9	24.31		1.69	5.46
	31.82	0.51	0.15406	0.9	16.27		3.78	7.77
	36.25	0.31	0.15406	0.9	24.69		1.64	4.51
	50.58	0.42	0.15406	0.9	20.77		2.32	3.91
	58.23	0.29	0.15406	0.9	30.70		1.06	2.32
3 Layer	21.32	0.25	0.15406	0.9	31.84	31.29	0.99	5.89
	30.20	0.25	0.15406	0.9	32.41		0.95	4.10
	36.32	0.21	0.15406	0.9	39.52		0.64	2.81
	50.51	0.25	0.15406	0.9	34.60		0.84	2.35
	60.17	0.51	0.15406	0.9	18.08		3.06	3.82

While the crystal size (from FESEM image) was 33.85, 21.21, 32 nm for samples a, b, and c respectively. This difference in the values from the XRD values is due to the interference between crystals and the lack of clarity in the imaging of the samples.

To study the elemental characterization, purity and elemental distribution, EDS and mapping tests were investigated as shown in figure (6). It could be noticed clearly that the prepared material exhibited high purity, hence no other elements rather than Zn and O were detected. A peak related to Au was also detected, which assigned to coating the sample with gold for testing FESEM. As well, the ratio of Zn:O was 53.4: 46.6 in the single-layer sample (figure 6 a). Meanwhile, an increase in the percentage of Zn:O 75.2: 24.8 when dipping cycles were become two-layer sample (figure 6 b). Finally, in the three-layer sample, the percentage was 90:10 as shown in figure (6 c). These results indicated that the elemental composition and the oxides state were strongly affected by the number of dipping times and thus the thickness.

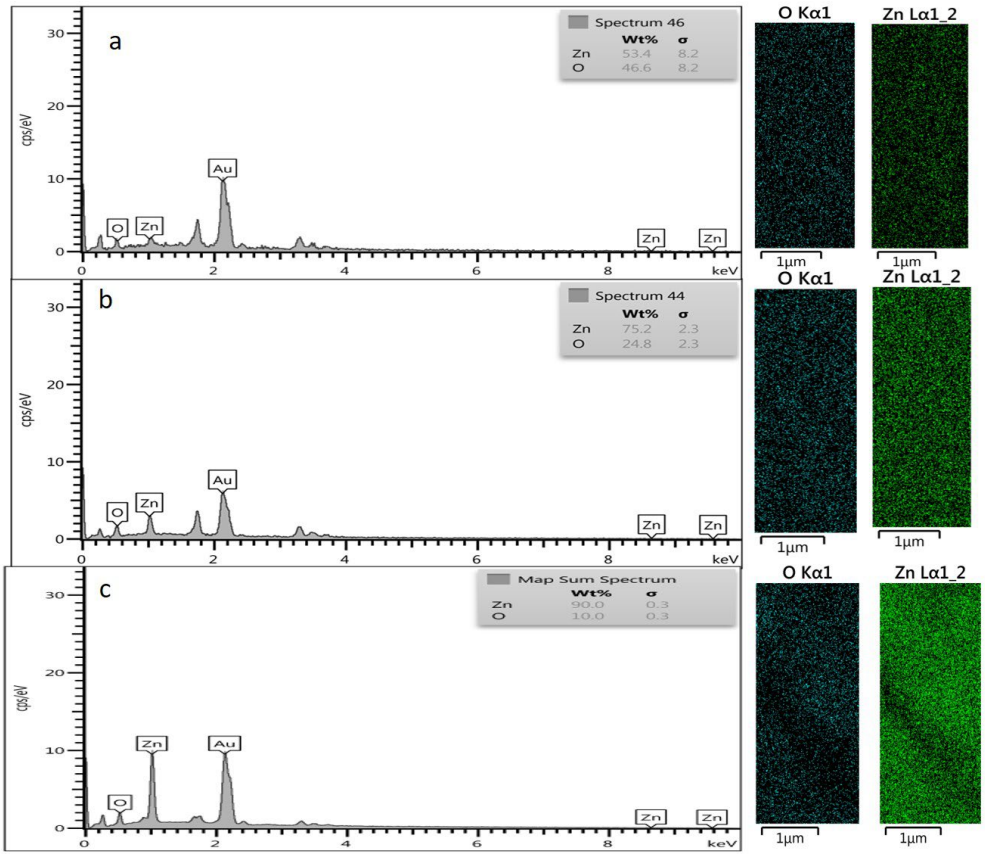

Figure (6). EDS and mapping test for a) 1 layer b) 2 layer

c) 3 layer.

Optical properties

The quality of the thin film could be controlled by several parameters such as concentration of Zinc acetates. Various characterizations could applied to investigate the quality of the prepared thin film. One of these important characterizations is the transparency. This is due to their application in several fields such as transparent conductive oxides (TCO). In this study, the transparency of the deposited ZnO thin films was studied. The investigations reveled that transparent ZnO thin films were produced at concentration of (0.1) M, as shown in figure (7). These results indicated that these films are suitable for TCO applications.

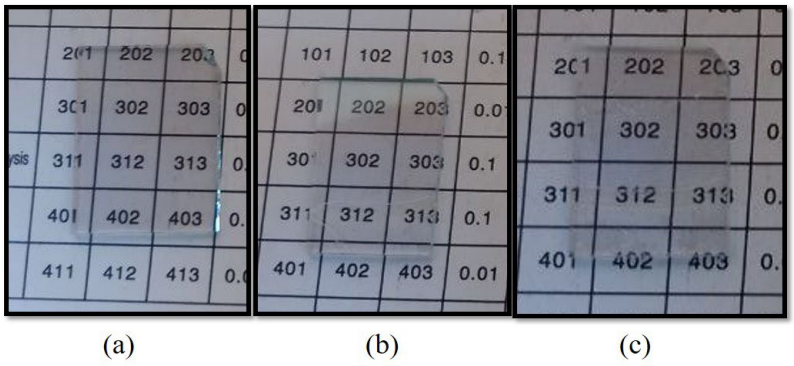

Figure (7). Photographs of transparent thin films a) 1 layer, b) 2 layer, and c) 3 layer.

One of the properties that was calculated is the energy gap of the thinfilm prepared using the relation between (E=hυ (eV)) and $(\alpha h\upsilon)^2$ $(eV/cm)^2$ as shown in figure (8). This figure shows that by increasing the number of coating times (increasing the thickness of the prepared thinfilm), the energy gap decreases. The one-layer sample was (E_g = 3.552 eV), the two-layer sample was (E_g = 3.277 eV), and the three-layer sample was (E_g = 3.229 eV).

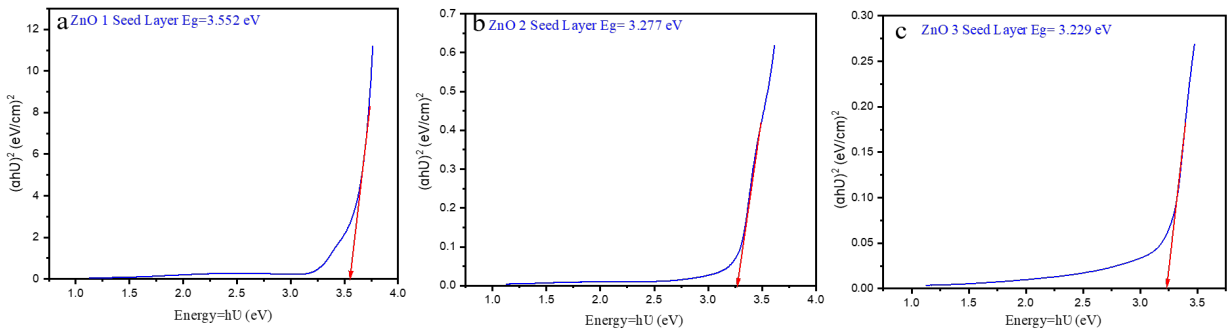

Figure (8). Energy gap for samples a, b, and c.

The optical transmittance of the prepared thinfilms was characterized. The results showed a high transparency around (80 – 87 %) as shown in figure (9). Through examinations of the prepared samples, it is clear that at low wavelength from 180 nm to 325 nm all samples have a low transparency which indicates the high absorbance. At 325 nm, an optical absorption edges were noticed clearly, which could be identified by the optical gap of ZnO. While, when the wavelength increased from 325 nm to 400 nm, transparency begins to gradually increase during this range. Finally, when the wavelength accessed visible light and NIR area, transmittance increased up to (80-87 %). Moreover, it is obvious that sample c showed less transmittance than the rest of the other samples. This could be attributed to the number of dipping, hence sample c was dipped three times which led to produce thicker layer and then lower transmittance compared to other samples which were dipped once or twice. This finding indicated that this preparation method represents an exciting method for fabricating ZnO thin films with controlled thickness.

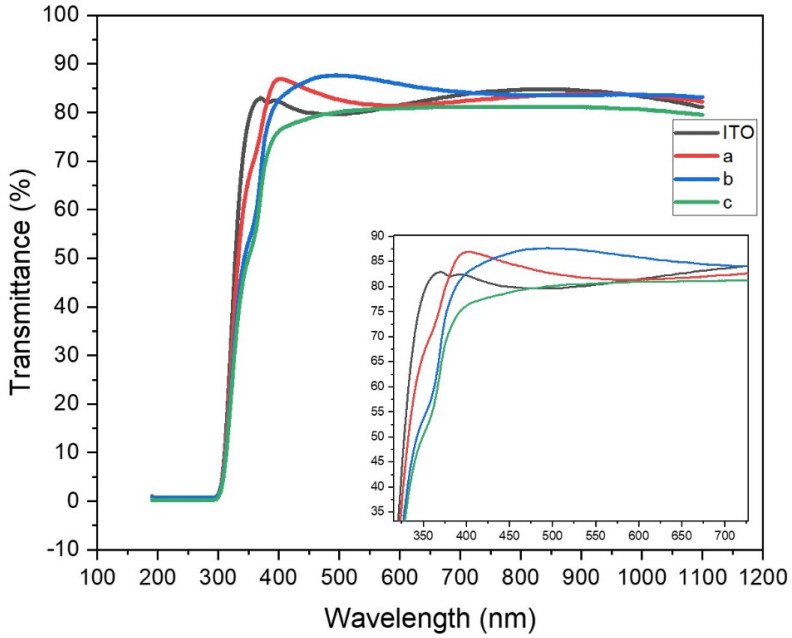

Figure (9). UV – Vis characterization of the prepared ZnO thin films for ITO substrate and seed layer a) 1 Layer, b) 2 Layer, and c) 3 Layer.

The I-V properties of ZnO thin films deposited on the ITO substrate were tested by measuring the voltage resulted from applying a variable current. The results confirmed that all the prepared thin films exhibited ohmic properties as shown in figure (10). The sheet resistance of samples (10 a) and (10 b) was not totally linear which indicated that the seed layer is not homogeneously covered the surface. Meanwhile, for sample c the sheet resistance increased linearly which displayed that the prepared thin film was homogeneous. Assuming that all other parameters remain constant, the sheet resistance is directly proportion with the film thickness[29]. In this work, the sheet resistance is inversely proportional to the thickness. This is due to the fact that more dipping cycles lead to higher thickness. In other word, the samples (10 a) and (10 b) exhibited less

thickness than sample (10 c) with inhomogeneous film. The uncontinued film has uncovering parts that act as resistance, which rise the sheet resistance.

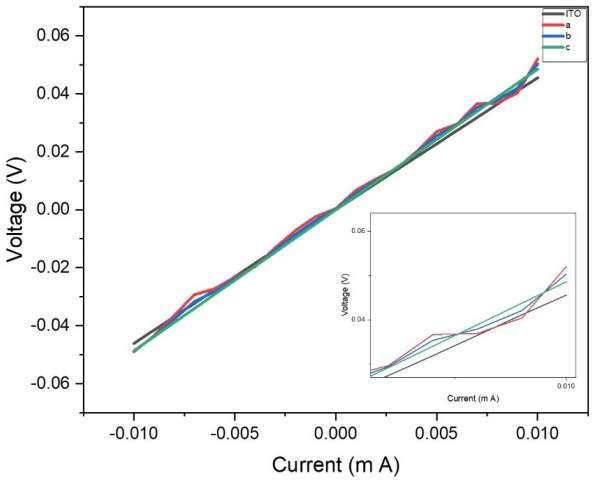

Figure (10). I-V characterization for bare ITO, samples a) 1 Layer, b) 2 Layer, and c) 3 Layer.

Table (2). Four point probe Method sheet resistance for samples with varying (concentration and dipping cycles).

Sample	Dipping cycles	$R_{ss}(\Omega\ sq^{-1})$
ITO	0	18.372
a	1	19.477
b	2	19.339
c	3	19.202

Through the electrical and optical examinations of the three samples, and by increasing the number of coating times, we notice an improvement and regularity in the electrical properties and a decrease in resistance (as showed in table 1). As for the optical properties, the increase in the number of coating times resulted in uniformity in the thin film and it has the same transparency figure (9 sample c). The uniformity of the electro-optical properties was caused by the homogeneity of the prepared thin film by increasing the number of coating times. The mobility of the carrier, which is affected by the crystalline and nanostructure of the polycrystalline material, was thought to explain this phenomenon. The increment in the resistivity depends on the crystallinity, thickness and grain size. With the (dip coating) approach, it can possibly build up more and more layers to reduce the sheet resistance of the transparent conductive electrode while

maintaining the lowest optical transmittance in the spectrum. The study of the optical and electrical properties and the reduction of the sheet resistance of the thin films in this paper lies in its use in the applications of transparent conductor oxides (TCO). It is highly conductive and transparent at the same time.

Mechanism

The characteristics of the thin films and their thickness depend on several factors such as immersion time, dragging speed, number of immersion times, solution formation, temperature, and environmental humidity [35]. The substrate is withdrawal vertically at a certain distance, then it dips at a certain speed from the solution so that the substrate will be wet with a thickness and the thinfilm will be formed soon when the substrate pulled out from the solution. The factors that affecting the thickness of the thin films (in addition to the above) the inclusion of surface tension along with the height of the membrane due to the effects of drying and separation pressure (or docking) and is important for films less than 1 micrometer thick [36]. The thickness of the thin film (λ) is calculated from the relationship (Landau_ Levich):

$$\lambda = 0.94 \frac{(\nu_o \eta)^{2/3}}{\gamma^{1/6}\sqrt{\rho g}} \qquad (4)$$

Where υ_o is the velocity of withdraw sample, γ is the surface tension of liquid at the position, g is the gravitational constant (9.81 m s^{-2}) and η is the viscosity of the liquid [37]. During pulling the substrate, the solution of the thin films begins to be attached to them, and the thickness of the layer depends on the speed at which the substrate is pulled, hence the slower the pulling, the thinner the coating layer [38,39].

CONCLUSION

A low cost (around 100 $) dip coating system was successfully set up. For testing the system, ZnO's thin films were deposited on ITO substrate at RT (± 23 ºC). The prepared thin films showed homogeneous distribution and particles size in nanoscale. Additionally, high transmittance hence that one-time dipping cycle exhibited a transmittance of 87% while dipping for 3 times showed less transmittance of 80 %. As for surface resistance, one dipping cycle showed higher surface resistance than the surface resistance value of the other samples. Thus, it can be concluded that this system can be considered as a low cost, facile and suitable to prepare thinfilms.

REFERENCES:

1. Dubowik, J.; Zał\keski, K.; Głowiński, H.; Gościańska, I.; *Phys. Rev. B* **2011**, *84*, 184438.

2. Sakamoto, K.; Kuwae, H.; Kobayashi, N.; Nobori, A.; Shoji, S.; Mizuno, J.; *Sci. Rep.* **2018**, *8*, 1.

3. Ji, C.; Liu, D.; Zhang, C.; Jay Guo, L.; *Nat. Commun.* **2020**, *11*, 1.

4. Azani, M.-R.; Hassanpour, A.; Torres, T.; *Adv. Energy Mater.* **2020**, *10*, 2002536.

5. Cai, C.; Jia, F.; Li, A.; Huang, F.; Xu, Z.; Qiu, L.; Chen, Y.; Fei, G.; Wang, M.; *Carbon N. Y.* **2016**, *98*, 457.

6. Aloui, W.; Ltaief, A.; Bouazizi, A.; *Superlattices Microstruct.* **2013**, *64*, 581.

7. Kulkarni, G. U.; Kiruthika, S.; Gupta, R.; Rao, K. D. M.; *Curr. Opin. Chem. Eng.* **2015**, *8*, 60.

8. Hecht, D. S.; Hu, L.; Irvin, G.; *Adv. Mater.* **2011**, *23*, 1482.

9. Goktas, S.; Goktas, A.; *J. Alloys Compd.* **2021**, *863*, 158734.

10. Chen, S.; Liu, F.; Xu, M.; Yan, J.; Zhang, F.; Zhao, W.; Zhang, Z.; Deng, Z.; Yun, J.; Chen, R.; others; *J. Colloid Interface Sci.* **2019**, *553*, 613.

11.**[S.d.]**, https://www.paint.org/coatingstech-magazine/articles/coatings-clinic-solvent-properties/.

12. Hussmann, E. K.; In *Optical Surface Technology* 1983.

13. Dubey, K. C.; Zaidi, A.; Awasthi, R. R.; *ACS omega* **2022**, *7*, 28946.

14. Sahoo, B.; Pradhan, S. K.; Mishra, D. K.; Sahoo, S. K.; Nayak, R. R.; Behera, D.; *Optik (Stuttg).* **2021**, *228*, 166134.

15.**[S.d.]**.

16. Pedersen, H.; Barry, S. T.; Sundqvist, J.; *J. Vac. Sci. \& Technol. A* **2021**, *39*, 51001. [https://doi.org/10.1116/6.0001125].

17. Foumani, A. A.; Förster, D. J.; Ghorbanfekr, H.; Weber, R.; Graf, T.; Niknam, A. R.; *Appl. Surf. Sci.* **2021**, *537*, 147775.

18. Peksu, E.; Karaagac, H.; *J. Alloys Compd.* **2021**, *862*, 158503.

19. Wang, Y.; Tang, B.; Gao, Y.; Wu, X.; Chen, J.; Shan, L.; Sun, K.; Zhao, Y.; Yang, K.; Yu, J.; others; *ACS omega* **2021**, *6*, 19238.

20. Saraf, C.; Barodiya, D.; **[s.d.]**.

21. Liao, C.; Wang, W.; Wang, J.; Han, L.; Qiu, S.; Song, L.; Gui, Z.; Kan, Y.; Hu, Y.; *J. Energy Chem.* **2021**, *56*, 1.

22. Ridha, N. J.; Alosfur, F. K. M.; Kadhim, H. B. A.; Ahmed, L. M.; *Mater. Res. Express* **2021**, *8*, 125013.

23. Sivakumar, P.; Akkera, H. S.; Reddy, T. R. K.; Bitla, Y.; Ganesh, V.; Kumar, P. M.; Reddy, G. S.; Poloju, M.; *Opt. Mater. (Amst).* **2021**, *113*, 110845.

24. Hameed, A. S.; Madlool, R. A.; Ridha, N. J.; Hussein, B. M.; Alosfur, F. K. M.; Tahir, K. J.; *Mater. Res.* **2022**, *25*,.

25. Das, H. T.; Vinoth, S.; Thirumoorthi, M.; Alshahrani, T.; Hegazy, H. H.; Somaily, H. H.; Shkir, M.; AlFaify, S.; *J. Inorg. Organomet. Polym. Mater.* **2021**, *31*, 2606.

26. Gurauskis, J.; Lohne, Ø. F.; Lein, H. L.; Wiik, K.; *J. Eur. Ceram. Soc.* **2012**, *32*, 649. [https://doi.org/https://doi.org/10.1016/j.jeurceramsoc.2011.10.009].

27. Machuno, L. G. B.; Oliveira, A. R.; Furlan, R. H.; Lima, A. B.; Morais, L. C.; Gelamo, R. V.; *Mater. Res.* **2015**, *18*, 775.

28. Kumar, K. D. A.; Ganesh, V.; Shkir, M.; AlFaify, S.; Valanarasu, S.; *J. Mater. Sci. Mater. Electron.* **2018**, *29*, 887.

29. Krebs, F. C.; Spanggard, H.; Kjær, T.; Biancardo, M.; Alstrup, J.; *Mater. Sci. Eng. B* **2007**, *138*, 106. [https://doi.org/https://doi.org/10.1016/j.mseb.2006.06.008].

30. Castillo-Vilcatomaa, D. A.; Loartea, S. J.; Fernandez-Chillccea, A. A.; Pastranab, E. C.; Pastranaa, R. Y.; **[s.d.]**.

31. Yohandri, Y.; Khairunnisa, K.; Ramli, R.; Zainul, R.; *Eksakta Berk. Ilm. Bid. MIPA (E-ISSN 2549-7464)* **2019**, *20*, 62.

32. Smith, P. M.; Carey, P. G.; Sigmon, T. W.; *Appl. Phys. Lett.* **1997**, *70*, 342.

33. Lee, D.; Pan, H.; Ko, S. H.; Park, H. K.; Kim, E.; Grigoropoulos, C. P.; *Appl. Phys. A* **2012**, *107*, 161.

34. Kang, J.-H.; Ying, G.; Cheng, Y.-C.; Kim, C.-S.; Lee, S.-H.; Yu, K.-M.; *J. Electr. Eng. Technol.* **2015**, *10*, 325.

35. Lončarević, D.; Čupić, Ž.; In *Industrial Applications of Nanomaterials*; Thomas, S.,; Grohens, Y.,; Pottathara, Y. B., org.; Elsevier, 2019.

36. Brinker, C. ~J.; Hurd, A. ~J.; Schunk, P. ~R.; Frye, G. ~C.; Ashley, C. ~S.; *J. Non Cryst. Solids* **1992**, *147–148*, 424. [https://doi.org/10.1016/S0022-3093(05)80653-2].

37. Sadegh-cheri, M.; **2020**.

38. Tong, Y.; Bohm, S.; Song, M.; others; *Austin J. Nanomedicine \& Nanotechnol.* **2013**, *1*, 1003.

39. Choy, K. L.; *Prog. Mater. Sci.* **2003**, *48*, 57. [https://doi.org/https://doi.org/10.1016/S0079-6425(01)00009-3].